ELSEVIER

Materials Science and Engineering A 457 (2007) 69–76

MATERIALS SCIENCE & ENGINEERING A

www.elsevier.com/locate/msea

Nucleation and growth kinetics in high strength low carbon ferrous alloys

C.S. Pande *, M.A. Imam

Materials Science and Technology Division, Naval Research Laboratory Washington, DC 20375-5000, United States

Received 4 October 2006; received in revised form 29 November 2006; accepted 13 December 2006

Abstract

Nucleation and growth kinetics, and age hardening behavior in high strength, low carbon ferrous alloy containing 1.2 wt% copper and a model alloy, Fe–1.2%Cu, have been studied with and without the presence of carbides. It is well known that after austenization and quenching, Cu is retained in solid solution. During subsequent aging, Cu initially appears as a coherent nanometer size spherical precipitates. These precipitates, difficult to detect by conventional transmission electron microscopy (TEM), have been evaluated by small angle neutron scattering (SANS) measurements. Longer aging transforms the Cu precipitates into incoherent particles which are easily detected by conventional TEM. A combination of techniques such as TEM, SANS, and hardness measurements have been used to study nucleation and growth kinetics of copper in both alloy systems. Direct measurement from TEM micrographs and integral transform of the SANS data were used to calculate the size distribution for a variety of aging conditions. Published by Elsevier B.V.

Keywords: Small angle neutron scattering (SANS); Copper precipitation; High strength low alloy steel (HSLA); Transmission electron microscopy (TEM)

1. Introduction

High strength low alloy steel (HSLA) plates have potential for use on US Navy ships [1]. The major reason for this is a possible cost reduction in fabrication. Compared with high yield (HY) steels, HSLA steel can be welded more easily and with much less process control. It is believed that the required properties needed for fabrication can be achieved by suitable heat treatment and processing [1]. Recent development in friction stir welding may also contribute to its future use. It is of interest, therefore, to consider in detail the nucleation of the copper precipitation and its growth in these HSLA steel as a function of heat treatment and relate such microstructure with mechanical properties [2].

Yield stress and Young modulus behavior on aging in this alloy shows that the yield stress increases rapidly with aging whereas the Young's modulus does not do so. Early experiments initially observed precipitates only in specimens aged for a long time. The precipitates are essentially pure fcc copper, the so-called ε phase. It was Hornbogen [3] who first suggested that the initial strengthening of Fe–Cu alloys is caused by the formation of coherent (bcc) copper clusters. This was confirmed indirectly by Lahiri et al. [4] using the Mossbauer technique. However, they were unable to obtain definite information on the size and number density of the clusters. Goodman et al. [5], determined these parameters for the early stage precipitation of copper in Fe–1.4% (atomic) Cu at 500 °C using field ion microscope (FIM). They found that the alloy reached its peak strength when the copper precipitates were on the average only 2.4 nm in size and still coherent. It should be noted that the term 'coherent' and 'incoherent' should be really considered as 'coherent' and "partially coherent". When coherent, the copper precipitates may not have only copper atoms but some other atoms may also be present. A more accurate term may be bcc copper and fcc copper precipitates.

As mentioned before, copper precipitates are nearly invisible in TEM (due to poor diffraction contrast) when they are fully coherent with the matrix [3,6]. However, they could still be characterized by small angle neutron scattering techniques (SANS) [7–9]. Other techniques that have been used are field ion microscopy [5,10–14], high-resolution transmission electron microscopy, and conventional transmission electron microscopy [6,15–17] for larger precipitates. Computer simulation [18] also can be useful. For a discussion of latest results see Ref. [19].

In our present studies the strength of the alloy as determined from micro hardness data is also found to peak, before the copper precipitates were visible in the electron microscope, i.e. before they had transformed from coherent bcc phase to incoherent fcc phase. The early stage of the precipitation is thus of technical as well as of scientific interest. One of the purpose of the present study was thus to try to obtain further evidence for a precipitation

* Corresponding author. Fax: +1 202 767 2623.
E-mail address: pande@anvil.nrl.navy.mil (C.S. Pande).

0921-5093/$ – see front matter. Published by Elsevier B.V.
doi:10.1016/j.msea.2006.12.043

stage preceding ε phase precipitation and obtain some further information of the mechanism of the evolution of the pre ε phase into the ε phase. In the present study, we have characterized both the coherent and incoherent copper precipitates with SANS and incoherent precipitates with TEM. Over 30 specimens have been analyzed for average size, size distribution and volume fraction as a function of aging conditions by TEM and SANS.

Apart from copper precipitation, a second type of precipitation is of importance in this material. It is the precipitation of carbides such as NbC. The transition metals, titanium, vanadium and niobium have a strong affinity for carbon and nitrogen in these steels and therefore form carbides and carbonitrides (since usually there is sufficient nitrogen present in these steels) [7]. It may thus be more appropriate to consider these carbide precipitates as NbC_xN_y—i.e. niobium carbonitrides with varying amounts of carbon and nitrogen. These precipitates can be present as extremely fine particles (6–10 nm), hence they are very effective in pining austenite (γ) grain boundaries. They, therefore, determine the austenite grain size. They, however, also complicate the study of copper precipitation by SANS.

Wagner et al. have presented the modeling of the precipitatiion kinetics in an Fe-Cu alloy (cf. section 5.7.6, p. 392 and also Fig. 5.12, p. 330 where they show magnetic and nuclear scattering data). In that kind of modeling they also discussed the structural phase transition (metastable coherent bcc to stable incoherent fcc ppts.) In fact, there they have assumed that the onset of the bcc → fcc transformation only depends on the radius of the Cu-ppts. and not on the aging conditions. Their paper used only SANS measurements but our paper using both SANS and TEM confirms their findings to a large extend.

2. Experimental

In order to separate the two precipitation kinetics in A710 steel, we designed a new alloy referred here as "model alloy" whose composition is given in Table 1. The composition of both the 'model' and the commercial alloy, A710 steel, used in this study is such that they exhibit essentially only copper precipitation for certain heat treatments, more so for the model alloy. By suitable selection of alloying elements, one can minimize carbide and nitride (or carbonitride) formation and thus study copper precipitation alone. Specimens of A710 steel having the two different compositions, one from a commercial lot and the second from the "model alloy", were cut to size of 25 mm × 12 mm × 2.5 mm. The samples were divided into two groups and each was given two different heat treatments. The first group was heated to 925 °C in an argon atmosphere and held there for 1 h followed by a water quench. The second group was heated to 700 °C for 100 h followed by a water quench. The samples were then aged at 500 °C in a salt bath for times ranging from 15 min to 100 h. The initial heat treatment was for solutionizing the specimens. The summary of the heat treatment procedure is given in Table 2. After aging, the samples were polished with #600 emery paper to remove surface oxide.

Small angle neutron scattering techniques were then used to characterize both coherent and incoherent precipitates in these steels. (SANS experiments reported here are preliminary and somewhat limited in scope, since they were in general in agreement with the results from Wagner et al. [8,9].) Two samples of 5 mm thickness were used in each SANS run. In addition to a different copper content, the copper precipitates and the surrounding ferrite (a) matrix exhibit different magnetization characteristics. Therefore, there is both a nuclear and a magnetic component to the SANS. Additionally, the matrix itself is magnetic. The SANS experiments, therefore, were done under a strong magnetic field affixed to the specimens and perpendicular to the incident beam. SANS intensity was measured both parallel and perpendicular to the magnetization of the specimen. (it has been shown in [8,9] the ratio between magnetic and nuclear scattering intensities can in fact give some information on the composition of the ppts. Since we were primarily interested in the size of the precipitates this ratio was not measured. In view

Table 1
Composition of the alloys in weight percent

Element	Model Alloy	Commercial Alloy
Fe	>97.4	>95.9
Cu	1.3	1.25
Ni	0.90	0.95
Cr	0.004	0.66
Mn	0.10	0.51
Si	0.30	0.34
Mo	0.006	0.21
Nb	0.004	0.010
Al	0.003	0.037
C	0.030	0.036
Sn	<0.002	0.016
N	0.0018	0.0092
S	0.0032	0.0085
V	<0.007	<0.007
P	0.0031	0.0045
Ce	<0.002	<0.002
Ti	<0.002	<0.002
Ca	0.0013	<0.0001

Table 2
Heat treatment of the alloy

Heat treatment	Aging (temperature)	Model alloy (aging time)	Commercial alloy (aging time)
925 °C for 1 h and water quench	500 °C	15 M	15 M
		20 M	20 M
		40 M	40 M
		70 M	70 M
		10 H	10 H
		50 H	50 H
		100 H	100 H
700 °C for 100 h and water quench	500 °C	15 M	15 M
		20 M	20 M[a]
		40 M	40 M
		70 M	70 M
		10 H	10 H
		50 H	50 H
		100 H	100 H

M = Minutes, H = Hour.
[a] Specimen not analyzed by SANS.

of the recent interest in the composition of these precipitates we plan to reconsider this issue later).

Consider a specimen containing precipitates with a given nuclear scattering length. If a strong and homogeneous magnetic field is applied to the specimen, all electron spins will align in one direction-perpendicular to the incident neutron beam. We can then measure the scattered neutron intensity parallel and perpendicular to the applied magnetic field. The scattering cross section parallel to the field will have only a nuclear scattering, while the one perpendicular will have both nuclear and magnetic components. The two components can thus be distinguished. For the present investigation we are concerned only with the nuclear component by using an appropriate magnetic field.

All SANS measurements reported here were made at the National Institute of Standards and Technology's (NIST's) SANS facility at Gaithersburg, Maryland. The sample-to-detector in the experiment was kept at the 3.6 m. In general sample/detector distance could be varied for optimizing the resolution in particular at low q but it was found to be not necessary for our purpose. The beam size was 8 mm in diameter and the wavelength was 0.6 nm. SANS was carried out by measuring the angular dispersion of an initially collimated beam of monochromatic neutrons on passing through a specimen and by using a position sensitive detector. The measurement time was approximately 3 h for each sample. The two-dimensional SANS profile of each sample was displayed on a color-graphics CRT terminal at NIST for background correction. The SANS profile was then corrected using the following relationship.

$$I_{cor} = (I_s - I_{sc}) - T_s(I_e - I_{ec})$$

where I_{cor} is the corrected intensity, I_s the intensity within sample, I_{sc} the intensity of the sample with cadmium, T_s the transmission through sample, I_{ec} the intensity with cadmium only, and I_e is the intensity without the sample.

The area imaging technique is quite suitable for observing many important details in the scattering pattern. However, a simpler procedure can be applied to the present problem by reducing the two-dimensional data to one-dimensional averaging. This is preferred since it improves the statistical accuracy, provided it can be ascertained that the details under consideration are not destroyed. In order to justify the use of circular averaging, specific angular segments of the data were first inspected by 'rectangular method'. A two-or-four-channel rectangle of data was first averaged horizontally, selecting data points from the bright spot, then along a 45° direction, selecting data mostly from the diffuse ring. It was observed that peaks of SANS profile from each sample obtained from the two orientations practically coincide. Thus, circularly averaged intensities are hereafter used in all analyses. The angular dispersion that results from penetrating the specimen can be related to the concentration and size distribution using diffraction theory. At the higher temperature, most of the copper is expected to go into solution, and will re-precipitate on subsequent aging. At the lower temperature (700 °C), only about 0.7% by weight out of the total copper of 1.2% by weight went into solution.

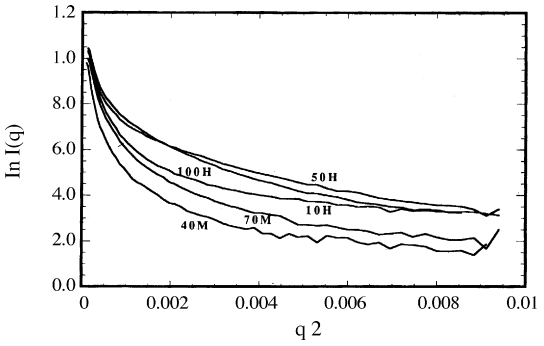

Fig. 1. Log SANS intensity vs. q^2 profile for commercial alloy heated to 700 °C for 100 h, water quenched and aged at 500 °C for different times as indicated.

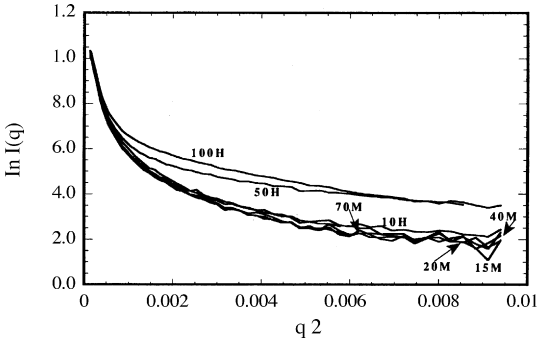

Fig. 2. Log SANS intensity vs. q^2 profile for model alloy heated to 700 °C for100 h, water quenched and aged at 500 °C for different times as indicated.

Typical SANS intensity profiles of log intensity versus q^2 (where $q = 4\pi \sin\theta/\lambda$, θ is the angle of scattering and λ is the wave length of the radiation) are shown in Figs. 1–4 for both the model and the commercial alloy for the heat treatments indicated. The rationale for plotting intensity profile in this fashion is that the initial slope of this curve (i.e. for $q^2 \rightarrow$ o) gives the 'Guinier radius', which can be related to the actual radius of the precipitates. However, we found that just obtaining Guinier radius was not very useful, as the slope was continuously changing with q. (Also almost all specimens contained undisolved larger precipitates, biasing the average size toward larger values). The shape of these curves clearly indicates that a distribution in sizes is present. These profiles were therefore analyzed for precipitate size distribution.

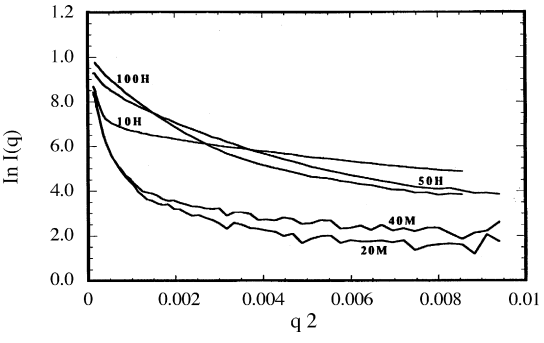

Fig. 3. Log SANS intensity vs. q^2 profile for model alloy heated to 925 °C for 1 h, water quenched and aged at 500 °C for different times as indicated.

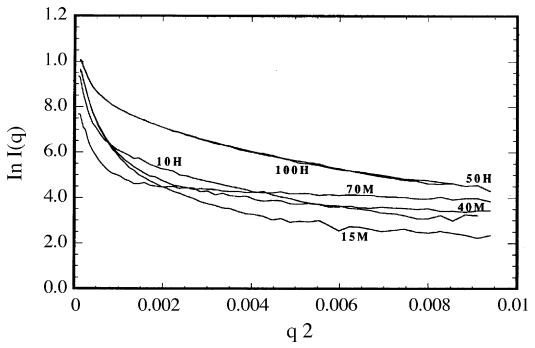

Fig. 4. Log SANS intensity vs. q^2 profile for commercial alloy heated to 925 °C for 1 h, water quenched and aged at 500 °C for different times as indicated.

3. Electron microscopy

A transmission electron microscopy (TEM) study was also conducted on the same or similar specimens. As pointed out before, the coherent copper precipitates are not expected to be visible using diffraction contrast in the transmission electron microscope because of the small mismatch, and hence weak diffraction contrast. However, at much larger aging times (and appropriate aging at temperatures) incoherent copper precipitates are easily visible in TEM, before aging, If all the copper is not dissolved during the solutionizing treatment, incoherent copper precipitates are also initially present.

Figs. 5 and 6 are two transmission electron micrographs of commercial HSLA steel. One micrograph relates to solutionizing at 700 °C for 100 h and then aging at 500 °C for 70 min (Fig. 5) whereas the other micrograph relates to solutionizing at 700 °C for 100 h and then aging at 500 °C for 10 h (Fig. 6). The copper precipitates are clearly visible where some of them are connected by dislocation (especially in the micrograph on the left). Fig. 7 shows a similar micrograph of the model alloy. Fig. 8 is a dark field transmission electron micrograph of the commercial HSLA steel aged for 97 h at 500 °C. Larger copper precipitates (more than 10 km in size) and smaller carbonitride

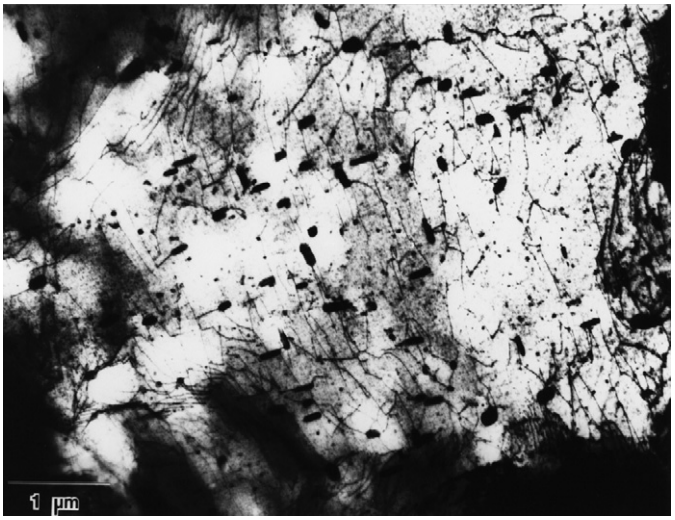

Fig. 5. A-710 (Commercial) solutionized at 700 °C for 100 h and aged at 500 °C for 70 min.

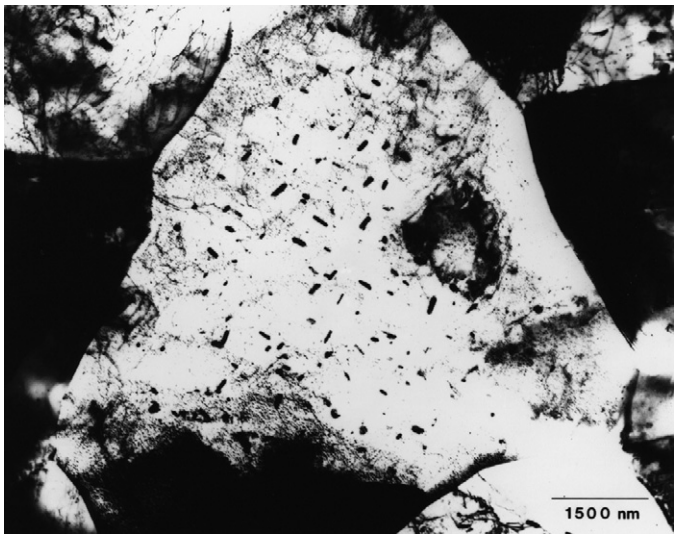

Fig. 6. A-710 (Commercial) solutionized at 700 °C for 100 h and aged at 500 °C for 10 h.

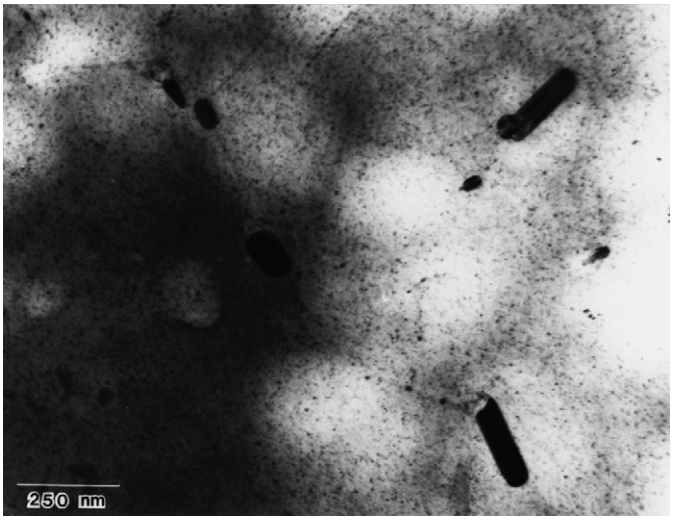

Fig. 7. A-710 (Model) solutionized at 700 °C for 100 h and aged at 500 °C for 100 h.

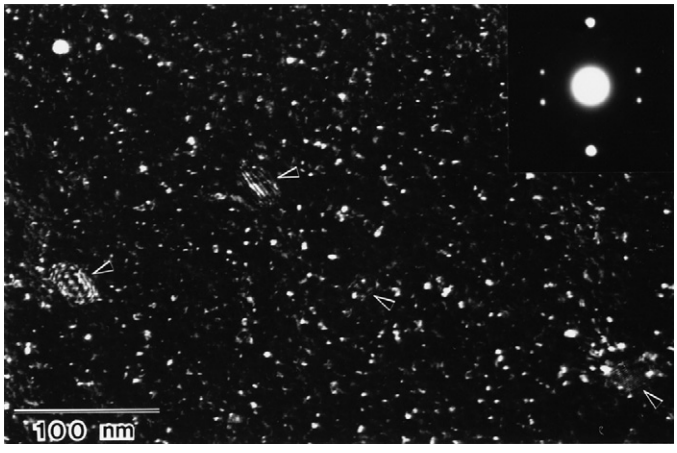

Fig. 8. Dark field transmission electron micrograph of the commercial HSLA steel aged for 97 h at 500 °C.

precipitates are also visible. The copper precipitates show Moire fringes with fine spacing.

The shape of the incoherent copper precipitates was found to be roughly spherical, as confirmed by tilting experiments, which showed little change in size as a function of tilting. A minimum of five foils were examined for each heat treatment condition. Larger precipitates are of course cylindrical as has been reported by other researchers. Histogram of precipitate sizes was obtained for each annealing condition by measuring the dispersoid size directly from the enlarged prints. Very small dispersoids (less then 10.0 nm) were not measured in this study because of the large error in their size measurement. The diffraction contrast pictures for such small precipitates may not provide a true indication of their size since this technique is influenced by strain distribution rather than actual size. Hence the error in measurement from the prints could have been substantial for these small dispersoid. Large oriented precipitates (cylindrical) in Figs. 5 and 6 are Cu ppts., originally present which did not dissolve during heat treatment.

In addition two other problems seriously complicated efforts to study Cu precipitation in these alloys. The first is oxidation in the original ingot. This shows up as an extremely fine, unresolvable dispersion of Fe_3O_4 in TEM specimens. It is not known to what extent the oxide affects Cu precipitation but the problem can be minimized by cutting slices from near the center of the ingot. A number of such slices were prepared, and electron diffraction from such center slices shows only faint Fe_3O_4 reflections.

A second problem proved more intractable. The usual electrolyte for thinning Fe is about 6% perchloric acid in ethanol (35 V, −40 °C). Using this electrolyte, specimens always showed a Cu precipitate with a size range of 2–10 nm, no matter how rapid the quench or what the subsequent heat treatment (up to 1 h at 650 °C). SAM analysis showed a high surface concentration of Cu on the TEM specimens, which dropped to the expected concentration after a brief sputter. These specimens then showed no Cu precipitation in the TEM. Clearly the precipitates were a surface effect generated during thinning. This could occur either by preferential removal of Fe during thinning, or by back plating after the voltage is cut off at the end of thinning.

Four methods have been tried to avoid this surface Cu accumulation. Removing the specimen from the electrolyte before cutting of the voltage could not be done quickly enough, resulting in too large a hole and no thin area. Etching in 5% perchloric acid in ethanol initially until only a little thin area was left, did not remove the Cu on the surface. Using a solution of about 30% phosphoric acid in water as electrolyte, we found no conditions, which produced good polishing, but eventually got some thin area (2 V at room temperature), which still showed the copper precipitate. Finally, ion milling the thinned specimen (obtained using the perchloric acid) does remove the copper from the surface, but even for 3 kV accelerating voltage Argon ions, some damage was introduced. We still believe that this approach is the only one by which any reliable results could be obtained. Using the electron diffraction pattern and dark field imaging one can ignore the damage and get the needed information on precipitate size and distribution (See Fig. 8).

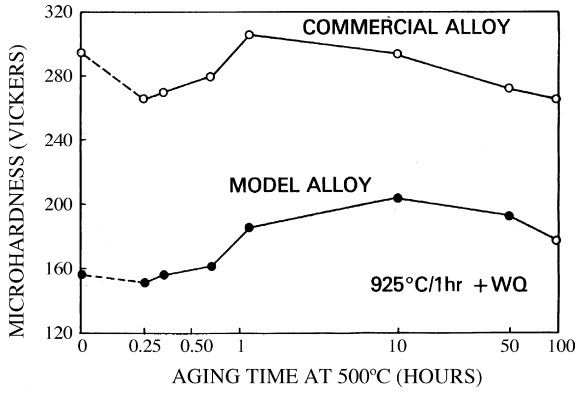

Fig. 9. Hardness vs. aging time plot.

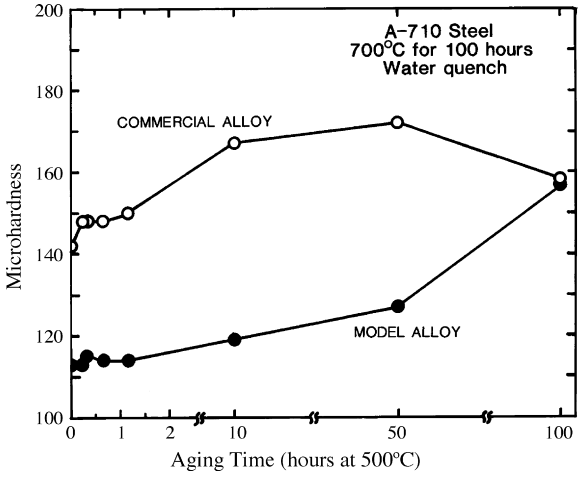

Fig. 10. Hardness vs. aging time plot.

4. Hardness measurements

Hardness measurements were made using a Vickers Micro hardness tester, in which a diamond pyramid in pressed into the sample under a 500 g load at high hardness levels and in measuring the hardness of a small region. In this experiment the Vickers micro hardness values are taken as an average of three measurements on each sample. Figs. 9 and 10 give the plots of hardness as a function of aging time.

5. Calculation of copper precipitate size distributions

The precipitate size distributions for larger sizes (>10 nm) could be obtained from the TEM micrographs. The exact form of the distribution, however, cannot be obtained since the part of the distribution for small size is not available. The transformation of the SANS intensity profiles to determine the precipitate size distributions is a more suitable method under these conditions. Ideally the most appropriate method is to guess a distribution such as Log Normal, calculate the intensity and adjust the distribution till it matches the intensity. Further refinement is possible using the more modern techniques such as Maximum entropy methods. We found the intensity signal not precise enough because of small amount of copper especially in the specimens

where due to incomplete homogenization large copper precipitates as seen by TEM were present. Since our aim is to obtain the average ppt. size the following two older methods were used to determine the copper precipitate size distributions from the SANS intensity profiles obtained in this study.

5.1. Vonks method

The first of these methods is a modification of a program developed by Vonk [20]. The program obtains the precipitate size distribution as a solution as a solution of the integral equation:

$$I(q) = K \int_0^{\infty} N(R) m^2 i_o(qR)\, dR \quad (1)$$

where $I(q)$ is the measured intensity, $N(R)$ the density of particles of radius R, m is the excess number of electrons in the particle, $i_o(qR)$ is the single particle scattering function which depends on the particle shape and radius and

$$q = 4p \sin q/1 \quad (2)$$

The algorithm used in Vonk's program is based on the assumption that the distribution function $N(R)$ obeys a modified Maxwellian form. This assumption places restrictions on the shape of the computed distribution function $N(R)$ and limits the applicability of this method to the specific cases where the assumption is very nearly obeyed, i.e. unimodal, nearly Maxwellian precipitate size distributions. We expected a unimodal distribution based on the work of previous researchers mentioned before.

The accuracy of the program itself was tested by running it through intensity profiles obtained from Raleigh's equation for single-size particles of known radius (5 nm in our case). The resulting size distribution curves were found to have very sharp peaks at the relevant radii, as they should. The method implemented by Vonk thus appears to work properly for the intensity profiles determined from size distributions that are known to obey the aforementioned assumptions. This method, however, should not be expected to reproduce size distributions that are, for example, bimodal or otherwise non-Maxwellian. These results, using Vonk's method, have been published elsewhere [21]. But, another method was used in order to verify the distributions generated by Vonk's program.

5.2. Brill's method

The second method for determination of the particle size distributions from the SANS data (and the method applied here) is the indirect transform method originally developed by Brill and Schmidt [22]. In the case of spherical particles, the unnormalized distribution function is given by:

$$N(D) = \frac{1}{D^2} \int_0^{\infty} [q^4 I(q) - P]\alpha(qD)\, dq \quad (3)$$

$$\text{where } \alpha(x) = [(1 - 8x^{-2}) \cos x] - \left[\frac{(4 - 8x^{-2}) \sin x}{x}\right] \quad (4)$$

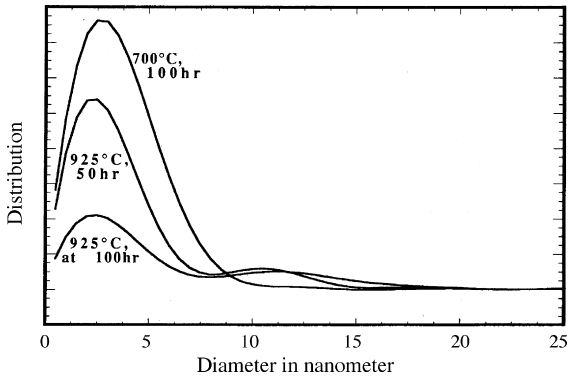

Fig. 11. Copper precipitate size distribution obtained from SANS for model alloy for two different homogenization temperatures (700 °C for100 h and 925 °C for 1 h) and water quenched in both. All aging was done at 500 °C for the time indicated.

Here P is the Porod constant given by :

$$P = \text{Limit}_{q \to \infty} q^4 [I(q)] \quad (5)$$

It characterizes the expected tendency of the scattering intensity to go as q^{-4} for large q. The advantage of the indirect transform method is that no functional form for the size distribution is assumed.

For our SANS data the intensity is extrapolated from q_{min} to 0, using Guinier's approximation:

$$I(q) = I_0 \exp(-\frac{1}{3} R_g^2 q^2) \quad (6)$$

where R_g is the Guinier radius.

$$\text{For large } q, \quad I(q) = C_4 q^{-4} + C_6 q^{-6} + C_8 q^{-8} \quad (7)$$

and $C_4 = P$ is the Porod constant and C_6 and C_8 are given by Brill and Schmidt [22].

Having extrapolated the SANS data to $q = 0$ and $q \to \infty$, using Eqs. (6) and (7), respectively, the particle size distribution is obtained using Eq. (4). It is found that if high enough values of q are not available experimentally, the q^{-4} behavior is not obeyed. If this was found to be the case, the data for those specimens

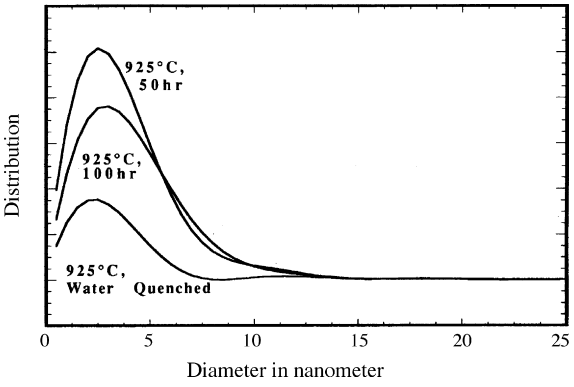

Fig. 12. Copper precipitate size distribution curves obtained from SANS for commercial alloy. Solutionization temperatures was 925 °C for 1 h, water quenched and aged at 500 °C for the time indicated.

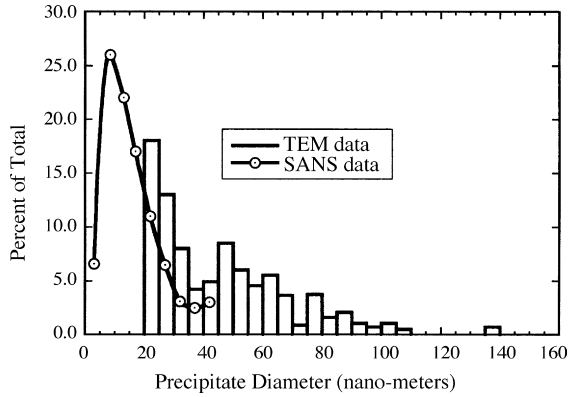

Fig. 13. An approximate size distribution plot combining the SANS and TEM data.

were not analyzed further. The number of precipitates per unit volume can also be calculated from the volume fraction and the distribution determined by SANS. Fig. 11 is a size distribution as obtained for model alloy based on SANS and Fig. 12 is a similar plot for the commercial alloy. The size distribution is seen to be spreading with aging time, though the peak remains almost unchanged. Finally Fig. 13 is an approximate size distribution plot combining both the SANS and TEM data. The peak in size for the SANS data is in the size range of coherent precipitates, as expected.

6. Discussion

In a standard system a precipitation reaction starts with the formation of critical size nuclei R^*, followed by growth and finally a competitive coarsening reaction. From the standard theory of nucleation [23] this requires an activation energy of nucleation such that:

$$\text{Nucleation rate proportional to } \exp\left(\frac{-4}{3}R^{*2}\sigma\right) \tag{8}$$

and $R^* = 2\sigma/G_v$, where G_v is the bulk free energy change per unit volume and σ is the interfacial energy per unit area of the precipitates.

More precisely steady-state homogeneous nucleation rate for a spherical critical nucleus:

$$J_{ss}^* = Z\beta^* N \exp\left(\frac{-4}{3}R^{*2}\sigma\right) \tag{9}$$

where Z is the Zeldovich non-equilibrium factor—corrects equilibrium nucleation rate for nuclei that grow beyond critical size β^* the rate at which single atoms are added to the critical nucleus N is the density of atomic sites available for nucleation.

The time-dependent homogeneous nucleation rate for a spherical critical nucleus is given by:

$$J_{ss}^* = Z\beta^* N \exp\left(\frac{-4}{3}R^{*2}\sigma\right) \exp\left(\frac{-\tau}{t}\right) \tag{10}$$

where τ is the incubation time. For a given system, Z, β^*, N and J_{ss}^* can all be evaluated if the appropriate ancillary data is available (e.g., diffusivity, etc.).

In the present case, σ is expected to be relatively small leading to a small R^* and hence a high nucleation rate. However, as the matrix is depleted in copper concentration, ΔG_V decreases and thus R^* increases suggesting that the nucleation rate drops drastically, and eventually the matrix gets further depleted of the solute. At latter stages one expects the coarsening phase to begin as described by LSW theory, leading to LSW type distributions. We did not, however, observed this. In fact the distributions obtained were closer to lognormal distributions. The reason for this behavior could be as follows:

After the embryos reach critical nucleus size, they immediately go into the growth regime. The activation energy for the growth process basically results from a combination of that due both to diffusion and that due to any interfacial/structural barriers (e.g., ledges, solute drag, etc.) and not from diffusion alone; the transition from "coherent to incoherent" precipitates probably occurs during growth (at least growth of the initial copper clusters). We believe that there are two competing effects that are applicable to the transition we are observing:

(I) First, accepting that the transition at the "peak size" in the distributions is occurring during growth; this transition could very well be due to the strain energy barrier due to growth of coherent ppts. (strain energy goes as cube of the size). This strain energy barrier is overcome by the "punching out" of misfit dislocations at the matrix: ppt. interface, resulting in the transition from full coherency to partial coherency. There are a number of older studies, which predict (and compare to experiment) the critical particle radius, r_{crit} at which this transition occurs. Thus, it seems to us that, it is r_{crit}, which may be important determining the peak. The equation for the critical radius is of the form:

$$r_{crit} = \frac{b}{16}\pi\varepsilon(1-\sigma)\left[\text{Ln}\left(\frac{8\sigma_{crit}}{b}\right) - 1 + \frac{(3-2\sigma)}{4(1-\sigma)}\right] \tag{11}$$

where b is the Burgers vector, ε the misfit and σ is the interfacial energy.

(For a good review of this topic, see pages, 339–365 of the review by Aaronson et al. [24], also see Ref. [89] of that review as well as Refs. [25,26].)

(II) The second point, which should be considered is that we are in addition dealing with a crystal structure change here. This further complicates the "transition" that we are observing; and corresponds to an initial clustering of Cu in the bcc ferrite, followed by the precipitation of a Cu phase of another crystal structure from the clusters. These two separate processes each have thermodynamic driving forces and, at least in the latter case, a barrier to nucleation, which must be considered, This transition may thus be considered in terms of the precipitation of fcc-Cu from the bcc-Cu clusters. (This is somewhat similar to what happens to carbon during the tempering of martensite.)

What is actually occurring during the "transition" manifested by our peak distribution is probably a combination of (I) and (II) above, with even further complications possible due to the possibility of some coarsening occurring.

Our paper describes an experimentally observed fact, that in the alloys studied the hardness reaches its peak, just before the copper precipitates in them had transformed from coherent bcc phase to incoherent fee phase. It is natural to ask what could be the micro mechanism(s) responsible for sensitivity of the hardness of low carbon ferrous alloys to coherency/incoherency of nanoscale precipitates? In this context, two recent papers may be cited. Zhao et al. [27] discuss the specific features of the dislocation structures near coherent, semi-coherent and incoherent precipitates in deformed ultra fine-grained alloys. Ovid'ko and Sheinerman [28], present the results of a theoretical model describing the nucleation of dislocations by nanoscale particles due to transformation of their coherency in deformed nanocomposites. In this work a new mechanism for nucleation of dislocation dipoles at nanoparticles (nanoinclusions) in nanocomposite solids is suggested and theoretically described. The mechanism represents the nucleation of a nanoscale dipole of 'non-crystallographic' partial dislocations. It is shown that the dislocations nucleated at nanoparticles can be emitted into a matrix in nanocomposites deformed at high mechanical stresses.

In particular, they propose that there exists a new alternative relaxation mechanism in nanoparticles under stress. This mechanism involves the non-local nucleation of a nanoscale dipole of 'non-crystallographic' partial dislocations (located at and near the nanoparticle-matrix interface) with a Burgers vector whose magnitude *grows* from zero to the Burgers vector magnitude b of a perfect lattice. The new mechanism involves a nanoscale ideal shear. According to their analysis of the energy characteristics of this mechanism effectively competes with the standard mechanism in wide ranges of applied stress and misfit values. Also, it is theoretically shown that nanoparticles can serve as sources of dislocations in nanoparticle-matrix nanocomposites deformed at high mechanical stresses.

Our experimental results are not inconsistent with these analyses but further experiments are needed.

In summary our results indicate that:

(i) The transition from coherent to incoherent copper precipitates may be discontinuous and presumably depends on the size of precipitates rather than on actual aging conditions.
(ii) The size distribution of copper precipitates are rather narrow and appears to be approximately lognormal.
(iii) The peak of the distribution does not shift appreciably during the early stages of precipitation.

Based on these results we summarise that the nucleation of the coherent bcc precipitates occur readily due to relatively low activation energy of nucleation and on aging they grow to a size roughly where a transition to fee structure takes place. The activation energy for this change is much higher as seen by the peak in the size distribution around this value ($\sim$5 nm). On further aging conventional coarsening should become significant leading to LSW type of size distribution which was not observed by us. Obviously we only observed the early stages of coarsening. Since hardening has already peaked aging studies for longer times were not performed.

Acknowledgements

The authors are grateful to Mr. L. E. Richards for hardness measurements and Dr. R. Vardiman and Mr. S. Smith for help with electron microscopy, and Dr. E. Dantsker for SANS analysis and Dr. George Spanos for critical comments on the manuscript. The authors are also grateful to Miss Mariam Ashraf for assistance in the preparation of this paper.

References

[1] P.W. Holsberg, J.P. Gudas, I.L. Caplan, Adv. Mater. Process. 1 (1990) 45.
[2] M.R. Krishnadev, A. Galibois, Metall. Trans. 6a (January) (1975) 222–224.
[3] E. Hornbogen, R.C. Glenn, Trans. AIME 218 (1960) 1064;
See also E. Hornbogen, Acta Metall. 10 (1962) 525;
E. Hornbogen, Trans. ASM 51 (1964) 120.
[4] S.K. Lahiri, D. Chandra, L.M. Swartz, M.E. Fine, Trans. AIME 245 (1965) 2496.
[5] S.R. Goodman, S.S. Brenner, J.R. Low Jr., Metall. Trans. 4 (1973) 263.
[6] C.S. Pande, S. Smith, L.E. Richards, in: G.W. Bailey (Ed.), Proceedings of 43rd Annual Meeting of Electron Microscopy Society of America, San Francisco Press, Inc., San Francisco, CA, 1985, p. 43.
[7] K. Osamura, H. Okuda, K. Asano, M. Furusaka, K. Kishida, F. Kurosawa, et al., ISIJ Int. 34 (1994) 346.
[8] R. Kampmann, R. Wagner, in: C. Janot, W. Petry, D. Richter, T. Springer (Eds.), Atomic transport and defects in metals by neutron scattering, Springer-Verlag, Berlin, 1986, p. 73, See also [9].
[9] R. Wagner, R. Kampmann, P. Voorhees, in: G. Kostorz (Ed.), Phase Transformations in Materials, Wiley-VCH, 2001, Chapter 5, pp. 309–408.
[10] G.M. Worall, J.T. Bushwell, C.A. English, M.G. Hetherington, G.W.D. Smith, J. Nucl. Mater. 148 (1987) 107.
[11] P.J. Pareige, K.F. Russell, M.K. Miller, Appl. Surf. Sci. 94/95 (1996) 362.
[12] M.K. Miller, K.F. Russell, P. Pareige, M.J. Starink, R.C. Thompson, Mater. Sci. Eng. A250 (1998) 49.
[13] N. Murayama, M. Sugiyama, T. Hara, H. Tamehiro, Mater. Trans JIM 40 (1999) 268.
[14] M. Murayama, Y. Katayama, K. Hono, Metall. Trans. A 30A (1999) 345.
[15] R. Monzen, M.L. Jenkins, A.P. Sutton, Philos. Mag. A A80 (2000) 711.
[16] P.J. Othen, M.L. Jenkins, G.W.D. Smith, W.J. Phythian, Philos. Mag. Lett. 64 (1991) 383.
[17] P.J. Othen, M.L. Jenkins, G.W.D. Smith, Philos. Mag. A A70 (1994) 1.
[18] F. Soisson, A. Barbi, G. Martin, Acta Metall. 44 (1996) 3789.
[19] D. Isheim, M.S. Galiano, M.E. Fine, D.N. Seidman, Acta Metall. 54 (2006) 841.
[20] C.G. Vonk, J. Appl. Crystallogr. 9 (1976) 433.
[21] C.S. Pande, M.A. Imam, L.E. Richards, C.L. Void, Proceedings of the International Welding Conference, vol. 1, New Delhi, India, 1987, p. 293.
[22] O.L. Brill, P.W. Schmidt, J. Appl. Phys. 39 (1968) 2274.
[23] K.C. Russell, Phase Transformation, ASM, Metals Park, Ohio, 1970, Chapter 6, p. 219.
[24] H.I. Aaronson, C. Laird, K.R. Kinsman, Phase Transformations, ASM, 1970, p. 313.
[25] W.A. Lesser, Philos. Mag. 19 (1969) 993.
[26] L.M. Brown, G.R. Woolhouse, Philos. Mag. 21 (1970) 329.
[27] Y.H. Zhao, X.Z. Liao, S. Cheng, E. Ma, Y.T. Zhu, Adv. Mater. 18 (2006) 2280.
[28] I. Ovid'ko, A.G. Sheinerman, J. Phys. Condens. Matter 18 (2006) L225–L232.